nature communications

Article

https://doi.org/10.1038/s41467-024-53992-x

Plasmid-encoded phosphatase RapP enhances cell growth in non-domesticated *Bacillus subtilis* strains

Received: 8 July 2024

Accepted: 28 October 2024

Published online: 05 November 2024

Check for updates

Manlu Zhu, Yiheng Wang, Haoyan Mu, Fei Han, Qian Wang, Yongfu Pei, Xin Wang & Xiongfeng Dai

The trade-off between rapid growth and other important physiological traits (e.g., survival and adaptability) poses a fundamental challenge for microbes to achieve fitness maximization. Studies on *Bacillus subtilis* biology often use strains derived after a process of lab 'domestication' from an ancestral strain known as Marburg strain. The domestication process led to loss of a large plasmid (pBS32) encoding a phosphatase (RapP) that dephosphorylates the Spo0F protein and thus regulates biofilm formation and sporulation. Here, we show that plasmid pBS32, and more specifically *rapP*, enhance growth rates by preventing premature expression of the Spo0F-Spo0A-mediated adaptive response during exponential phase. This results in reallocation of proteome resources towards biosynthetic, growth-promoting pathways without compromising long-term fitness during stationary phase. Thus, RapP helps *B. subtilis* to constrain physiological trade-offs and economize cellular resources for fitness improvement.

In nature, microbial cells must tightly couple gene expression with cell growth to constantly adapt to various environments[1,2]. Rapid growth is a fundamental concern of microbes and is crucial for population fitness[1,3–5]. However, the nutrient availability is often highly fluctuating in the natural niches of bacteria[6–10], and hence bacterial cells must employ sophisticated adaptive response to cope with severe nutrient limitation[11,12]. Therefore, in addition to the trait of growth, alternative physiological traits such as adaptability and survivability are also crucial for bacterial fitness[8,10,13–17]. Therefore, the gene regulation network of bacterial cells inevitably needs to support both the growth trait as well as other physiological traits[18,19]. Nevertheless, it is fundamentally challenging for bacterial cells to optimize these traits simultaneously as the gene repertoires for different traits (e.g., growth versus survival) are largely separated from each other[11,20] and thus have natural conflicts of resource allocation[21–23].

Recent studies have shown that the proteome investment on alternative traits could be substantial even during exponential stage, which limits the cellular budget for cell growth and results in trade-offs[10,19,24,25]. For example, when encountering poor nutrient conditions, *E. coli* cells harboring higher basal levels of alarmone (p)ppGpp and cAMP gain increased adaptability and stress response at the cost of reduced growth rate[9,10,18]. Therefore, bacterial cells do not always achieve growth maximization and could spare some "growth capacity" in some cases[18,26]. Similarly, growth acceleration by genetic perturbation or adaptive evolution might occur at the cost of reduced survivability, drug tolerance or adaptability[27–29]. The fundamental trade-off between cell growth and other important traits thus poses a natural challenge for microbial cells to implement resource allocation decisions. It remains unclear whether bacteria could somehow constrain or avoid such trade-offs to minimize the unnecessary resource preemption by alternative physiological traits from growth trait during exponential stage, namely, achieving need-based regulation of resource allocation.

Here we focused on the growth physiology of model Gram-positive bacterium *B. subtilis*, for which the growth control strategy still remains poorly understood. The laboratory domesticated strain 168, generated by X-ray treatment of the ancestral Marburg strain in 1940s[30], is not only the earliest sequenced model gram-positive

State Key Laboratory of Green Pesticide; Hubei Key Laboratory of Genetic Regulation and Integrative Biology, School of Life Sciences, Central China Normal University, Wuhan, PR China. e-mail: daixiongfeng@ccnu.edu.cn

bacterium[31] but also the most intensively studied object in the *B. subtilis* community due to its high amenability to genetic manipulation[32,33]. Compared with its ancestral Marburg strain NCIB 3610 (=ATCC 6051)[30], strain 168 has acquired a few mutations in related genes such as *sfp*, *swrA*, *trpC*, and *gudB*, and is thus defective in certain social behaviors such as biofilm formation and swarming motility[30,34]. Moreover, strain 168 has lost the pBS32 endogenous plasmid of the ancestral Marburg strain. These genetic differences raise the fundamental issue of to what extent strain 168 can really represent the growth physiology of its ancestral *B. subtilis* strain[35]. In this work, we identify a global strategy of the ancestral *B. subtilis* strain to achieve rapid growth without compromising long-term fitness by employing need-based regulation of resource allocation, which has been lost in the widely-used domesticated *B. subtilis* strain.

Results

rapP in pBS32 plasmid encodes a growth accelerator in *B. subtilis*

We first compared the growth rates of three *B. subtilis* strains including the wild type 168 strain, its ancestral NCIB 3610 strain and the NCIB 3610-derived DK1042 strain. DK1042 strain could be used as a substitute of NCIB 3610 strain with the only minor genetic difference being that the former one carries a Q12L mutation in the *comI* gene[36], locating at the endogenous pBS32 plasmid. Therefore, DK1042 strain is more amenable to genetic modification owing to its higher natural transformation efficiency than NCIB 3610 strain[36]. These three strains displayed the same growth rates in LB rich medium (Fig. S1). In contrast with LB medium, the domesticated 168 strain exhibited much lower growth rates than NCIB 3610 and DK1042 strains on various carbon sources including the preferred carbon source, glucose (Figs. 1A and S2A, B). Given that 168 strain has lost the endogenous pBS32 plasmid, we then looked into the growth of DS2569 strain[36], which was the pBS32-cured (ΔpBS32) NCIB 3610 strain (Fig. 1B). DS2569 strain displayed comparable growth rates with 168 strain, being also much lower than the growth rates of NCIB 3610 and DK1042 strains (Figs. 1C and S2C, D), suggesting that the reduced growth of strain 168 was mainly attributed to the loss of pBS32 instead of the few mutations in chromosome. This result is counterintuitive as it is proposed that the extrachromosomal plasmids often confer fitness costs on the host[37,38], suggesting that pBS32 plasmid might bear some potential growth accelerators.

Only a few genes in pBS32 have currently been characterized and the physiological function of this plasmid still remains unclear[35]. It has recently been shown that the deletion of *rapP* gene in pBS32 could negatively affect the growth rate of 3610 strain[39]. We thus next sought to investigate the *rapP* gene, encoding a Rap-family phosphatase that targets Spo0F and acts as an inhibitor of biofilm formation[35,40]. Strikingly, DS7906 strain (Δ*rapP*) displayed similar slow growth rates with the DS2569 (ΔpBS32) strain (Figs. 1C and S2C, D) and RapP complementation could fully restore the reduced growth rate of DS7906 strain (Fig. S3, pink), suggesting that the *rapP* gene itself was enough to account for the growth acceleration effect of pBS32. We note that complementation with RapP E49A, the phosphatase inactive form[40], could also (albeit not fully) restore the slow growth of DS7906 strain (Fig. S3, orange), suggesting that not only the

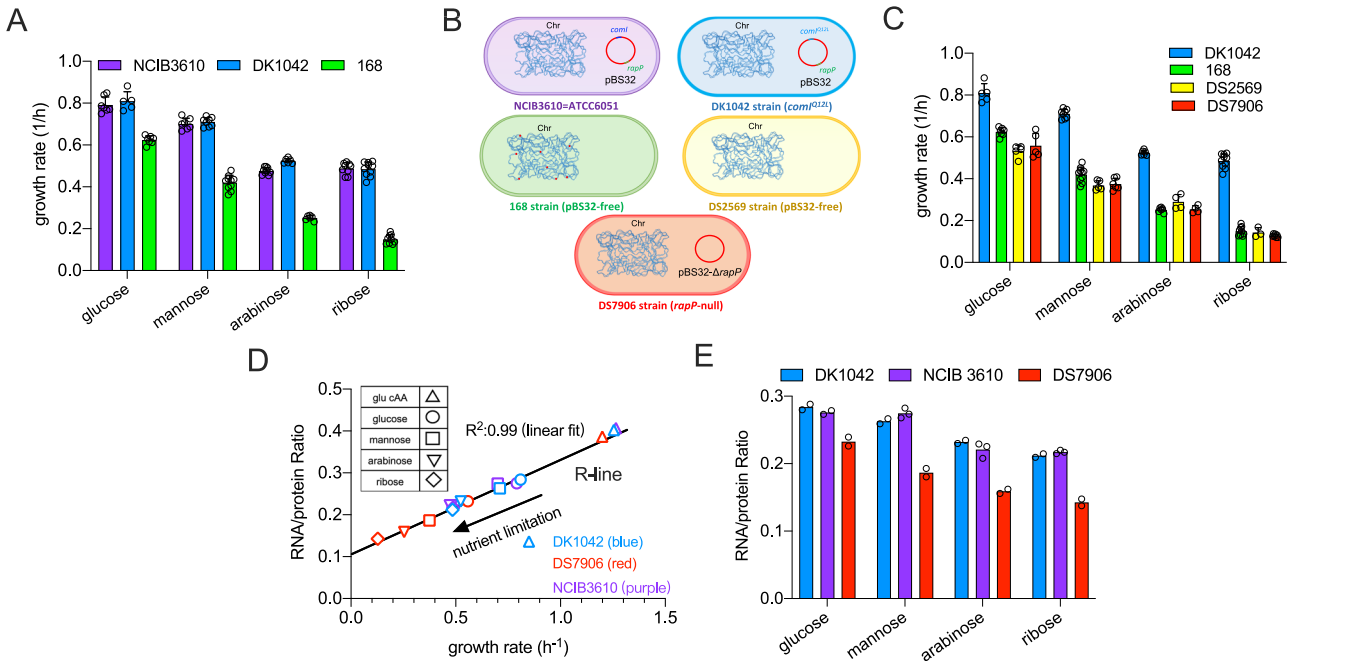

Fig. 1 | The growth physiology of undomesticated and domesticated *B. subtilis* strains. A The growth rates of NCIB 3610, DK1042, and 168 strains on various carbon sources. Data are presented as the mean values ± standard deviations (SD) of several biological replicates (for NCIB 3610 strain: $n = 7$ for glucose and mannose; $n = 9$ for arabinose and ribose; for DK1042 strain: $n = 5, 8, 6, 10$ for glucose, mannose, arabinose and ribose, respectively; for 168 strain: $n = 7, 10, 6, 9$ for glucose, mannose, arabinose and ribose, respectively). **B** Schematics of several *B. subtilis* strains used in this study. "Chr" is short for chromosome. NCIB 3610, DK1042, DS2569, and DS7906 share the same sequence of chromosomes while the domestical 168 strain carries additional mutations (represented by red points) in some chromosomal positions such as *sfp*, *swrA*, *trpC*, and *gudB*. **C** The growth rates of DK1042, 168, DS2569, and DS7906 strains on various carbon sources. Data of DK1042 and 168 are the same as (**A**). Data are presented as the mean values ± standard deviations (SD) of several biological replicates (for DS2569: $n = 5, 5, 4, 3$ for glucose, mannose, arabinose and ribose, respectively; for DS7906 strain: $n = 5, 6, 4, 7$ for glucose, mannose, arabinose and ribose, respectively). **D** Correlation of RNA/protein ratios versus growth rates for DK1042, NCIB 3610, and DS7906 strains under various nutrient conditions. Data of DK1042 and NCIB 3610 strains almost completely overlap with each other. **E** Comparison of RNA/protein ratios of DK1042, NCIB 3610, and DS7906 strains on different carbon sources. Individual data points are from different biological replicates. ($n = 3$ for NCIB 3610 on arabinose and ribose and $n = 2$ for all the rest conditions). Source data are provided as a Source Data file.

phosphatase activity but also some other effects (e.g., the direct binding to Spo0F[40]) contribute to the growth acceleration effect of RapP. We then measured the ribosome content of *B. subtilis* as ribosome synthesis lied at the core of bacterial growth control[2,4,41,42]. The RNA/protein ratio[2,43], a proxy of ribosome content, displayed the same linear correlation (R-line) with growth rate for DK1042, NCIB 3610, and DS7906 strains under various nutrient conditions (Fig. 1D). However, DK1042 and NCIB 3610 strains possessed higher ribosome content than DS7906 strain on all carbon sources alongside the R-line (Fig. 1D, E), suggesting that RapP could allow cells to devote more resources to biosynthetic pathways to support higher growth rates.

Growth acceleration effect of *rapP* depends on Spo0F-Spo0A signaling

When *B. subtilis* encounters harsh environments such as nutrient starvation or enters into stationary phase, cellular sensor kinases such as KinA and KinB are activated and further activate the master regulator Spo0A via the Spo0F-Spo0B-Spo0A phosphorelay[44]. The active phosphorylated form of Spo0A, Spo0A-P, further activates various adaptive processes such as cannibalism, competence, biofilm formation and ultimately, sporulation[44–47]. RapP, as a Rap-family phosphatase which is capable of targeting Spo0F[40,48,49], could regulate certain social behaviors of *B. subtilis* such as biofilm formation via interfering with the Spo0F-Spo0A signaling pathway[35,40]. We found that the knockout of *spo0F* or *spo0A* substantially increased the growth rates of DS7906 strain on various carbon sources (Figs. 2A and S4), as similarly observed in the case of 168 strain due to resource re-allocation from Spo0A-mediated survival and adaptive pathways to biosynthetic pathways (Fig. 2B)[27]. In contrast, *spo0F* or *spo0A* knockout only marginally affected the growth rates of DK1042 strain (Fig. 2C). As a result, in both *spo0F*-null and *spo0A*-null backgrounds, the growth difference between DK1042 (*rapP*$^+$) strain and DS7906 (Δ*rapP*) strain completely disappeared (Fig. S5), strongly suggesting that the growth acceleration effect of *rapP* attributes mainly to its interference of Spo0F-Spo0A signaling pathway, which could mimic the effect of *spo0A* deletion[27].

The effect of *rapP* on the expressions of sporulation genes

We next wondered how *rapP* could quantitatively affect the expressions of downstream genes of Spo0F-Spo0A signaling pathway. One of the central physiology processes located downstream of Spo0F-Spo0A signaling pathway is sporulation, a crucial adaptive strategy of *B. subtilis* in response to nutrient starvation[44,45]. qPCR analysis showed that the absence of *rapP* indeed stimulated the expressions of Spo0A-dependent sporulation genes such as *spoIIE, spoIIGA, spoIIAA*, and *sigE* in DS7906 strain compared with the *rapP*$^+$ DK1042 strain during exponential stage (Fig. 3A). We further systematically measured the promoter activities of *spoIIE* and *spoIIGA* using *lacZ* reporter assay to monitor the fluctuation of Spo0A activity during exponential stage under various nutrient conditions. Since the basal promoter activities of sporulation genes were very low during exponential stage even in poor nutrient conditions, *lacZ* reporter assay was based on a sensitive fluorescent substrate (see Section "Methods"). The promoter activities of *spoIIE* and *spoIIGA* in DS7906 strain exhibited a strong negative relation with growth rates on different carbon sources (red symbols in Fig. 3B, C). In contrast, the promoter activities of *spoIIE* and *spoIIGA* in DK1042 strain were largely maintained at basal levels (blue symbols in Fig. 3B, C), suggesting that RapP effectively suppressed Spo0A activity and further minimized the leaky expressions of Spo0A-dependent sporulation genes in *B. subtilis* during exponential stage. The strong growth-rate dependences of *spoIIE* and *spoIIGA* expressions were also observed in the wild type 168 strain which was also devoid of *rapP* (Fig. 3D, E, red symbols) but certainly compromised in the *spo0A*-null background (Fig. 3D, E, green symbols). The negative growth-rate dependent expression of sporulation genes supports that Spo0A activity undergoes marked fluctuations under different growth rates and increased even during slow exponential growth (before growth cessation), which is presumably the result of a "passive regulation" in which the release of RNA polymerase from rRNA synthesis during slow growth promotes *spo0A* transcription and further the production of active Spo0A-P[50].

The effect of RapP on proteome allocation in *B. subtilis*

To test the global effect of RapP on gene expression, we next systematically investigated the proteome allocation of *B. subtilis*. We compared the proteomes of exponentially growing DK1042 and DS7906 strains in both mannose and ribose media using 4D label-free mass spectrometry[51], which could capture over 2500 individual proteins of *B. subtilis* with high reproducibility (Supplementary data 1 and 2, Fig. S6). Heatmap analysis showed that the presence of RapP indeed reshaped the global gene expression pattern of *B. subtilis* (Fig. 4A, B). A visualization of cellular resource allocation by proteomaps website (https://proteomaps.net)[52] showed that DK1042 strain had a higher investment on ribosome biosynthesis but a lower investment on the biosynthesis of secondary metabolites (e.g., surfactin and other antibiotics) than DS7906 strain[53,54](Fig. 4C). Similar result could be observed when comparing the fast-growing DK1042 cells with the slow-growing DK1042 cells in two nutrient conditions (Fig. S7A). We further quantified the mass fractions of various functional proteome sectors of *B. subtilis* (Figs. 4D, E and S7B, Supplementary data 2–4). Although RapP had been primarily proposed to be a biofilm inhibitor[35], the proteome fractions of biofilm-related proteins were generally low and not quite affected by *rapP* knockout during exponential growth (Fig. S8), suggesting that the growth effect of RapP was not related to its regulation of biofilm formation. We then looked into the "core biosynthetic sector" of proteome that included various biosynthetic pathways supporting biomass growth. Among them, glycolysis and TCA cycle are central catabolic pathways that are responsible for cellular energy generation[55] as well as producing catabolic precursors for the subsequent anabolism[10]; amino acid (AA) biosynthesis and nucleotide (NT) biosynthesis are key anabolic pathways to supply amino acids and nucleotides[8]; ribosomes, ribosome (Rb)-affiliated proteins and tRNA charging proteins are directly engaged in protein synthesis[56]. Compared with the slow-growing DS7906 strain, DK1042 strain had a higher proteome investment on the core biosynthetic sector in both mannose and ribose media (Fig. 4F, G), being consistent with the result of RNA/protein ratio (Fig. 1D, E).

Proteome allocation constraint is fundamentally related to the growth control of bacteria[1,4]. It is intriguing that the ancestral *B. subtilis* strain has more cellular resources devoted to biosynthetic pathways to support faster growth. Then we wondered where did these extra resources come from? Given that RapP interferes with the Spo0F-Spo0A signaling pathway, we then looked into those major adaptive response pathways such as sporulation, surfactin biosynthesis, oligopeptide uptake, antibiotic biosynthesis, utilization of alternative nutrients, proteolysis, and response to toxicants (Supplementary data 3 and 4). DK1042 strain had substantially lower proteome investment on those major adaptive response pathways than DS7906 strain in both mannose and ribose media (Figs. 4H, I and S9). Moreover, the levels of some other minor sectors of adaptive response pathways such as cannibalism[46], competence[57], and glycogen biosynthesis[58], although being low in absolute abundances, were also downregulated in DK1042 strain compared with DS7906 strain (Fig. 4J). Therefore, compared with DS7906 strain, DK1042 strain achieves faster growth by allocating more cellular resources to fuel the biosynthetic pathways via turning down its cellular budget on adaptive pathways, as shown in Fig. 4K. These results are consistent with the effect of *spo0A* knockout on proteome

https://doi.org/10.1038/s41467-024-53992-x

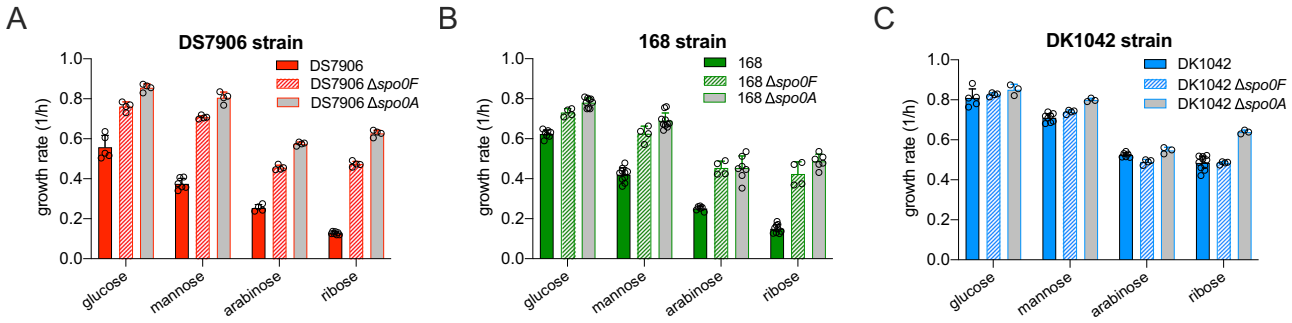

Fig. 2 | The effect of *spo0F* or *spo0A* knockout on the growth of DS7906, 168, and DK1042 strains. A The effect of *spo0F* or *spo0A* knockout on the growth rates of DS7906 strain on different carbon sources. Data are presented as the mean values ± standard deviations (SD) of several biological replicates. $n = 5, 6, 4, 7$ on glucose, mannose, arabinose and ribose, respectively for DS7906 strain; $n = 4$ for all the conditions of *spo0F*-null and *spo0A*-null strains. **B** The effect of *spo0F* or *spo0A* knockout on the growth rates of 168 strain on different carbon sources. Data are presented as the mean values ± standard deviations (SD) of several biological replicates. $n = 7, 10, 6, 9$ on glucose, mannose, arabinose and ribose, respectively for wild type 168 strain. $n = 4$ for all the conditions of *spo0F*-null strain. $n = 9, 10, 7, 6$ on glucose, mannose, arabinose and ribose for *spo0A*-null strain. **C** The effect of *spo0F* or *spo0A* knockout on the growth rates of DK1042 strain on different carbon sources. Data are presented as the mean values ± standard deviations (SD) of several biological replicates. $n = 5, 8, 6, 10$ on glucose, mannose, arabinose and ribose, respectively for DK1042 strain. $n = 4$ and 3 for *spo0F*-null strain and *spo0A*-null strain, respectively. Source data are provided as a Source Data file.

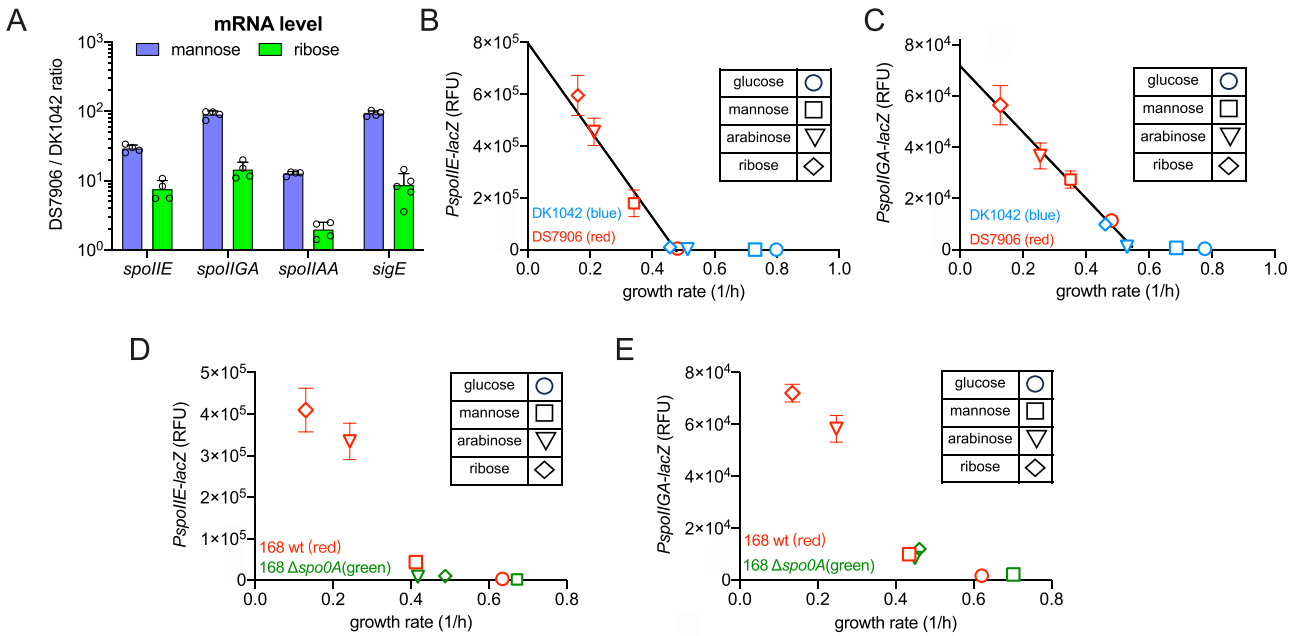

Fig. 3 | The effect of RapP on the expressions of sporulation genes. A Relative mRNA levels of four sporulation genes in DS7906 strain compared with DK1042 strain growing in mannose and ribose media, respectively. Data are presented as the mean values ± standard deviations (SD) of several biological replicates. $n = 4$ for all the conditions except in the case of *sigE* data on ribose, for which $n = 5$. **B** Growth-rate dependent promoter activities of *spoIIE* gene in DK1042 and DS7906 strains. Data are presented as the mean values ± standard deviations (SD) of several biological replicates. $n = 3$ and $n = 4$ for DK1042 and DS7906 strain, respectively. **C** Growth-rate dependent promoter activities of *spoIIGA* in DK1042 and DS7906 strains. Data are presented as the mean values ± standard deviations (SD) of four biological replicates ($n = 4$). **D** Growth-rate dependent promoter activities of *spoIIE* gene in wild type 168 and its *spo0A*-null strains. Data are presented as the mean values ± standard deviations (SD) of three biological replicates ($n = 3$). **E** Growth-rate dependent promoter activities of *spoIIGA* gene in wild type 168 and its *spo0A*-null strains. Data are presented as the mean values ± standard deviations (SD) of several biological replicates. $n = 3$ for all the data points. The LacZ reporter activities were measured by a fluorescent MUG substrate (see "Methods") and expressed as relative fluorescence units (RFU). Source data are provided as a Source Data file.

allocation[27] and confirm that the presence of RapP in ancestral strain, via targeting Spo0F-Spo0A signaling pathway, promotes cell growth by shifting cellular resources from Spo0A-mediated adaptive pathways to biosynthetic pathways. Systematically, for the four conditions studied here (two strains on two carbon sources), we could see clearly that the levels of core biosynthetic sector increased linearly with increasing growth rates while the levels of adaptation sector exhibited the opposite trend (Fig. 4L). Taken together, we concluded that the absence of RapP stimulated the overexpression of adaptive response pathways at the cost of reduced cellular investment on biosynthetic pathways, ultimately resulting in the reduced growth rate of *rapP*-null *B. subtilis* (illustrated in Fig. 4M).

Need-based activation of sporulation pathway in the ancestral *B. subtilis*

A potential problem associated with the increased growth rate of the ancestral *B. subtilis* is a compromise of fitness during starvation stage due to a lower investment on adaptive response, which is remarkable

https://doi.org/10.1038/s41467-024-53992-x

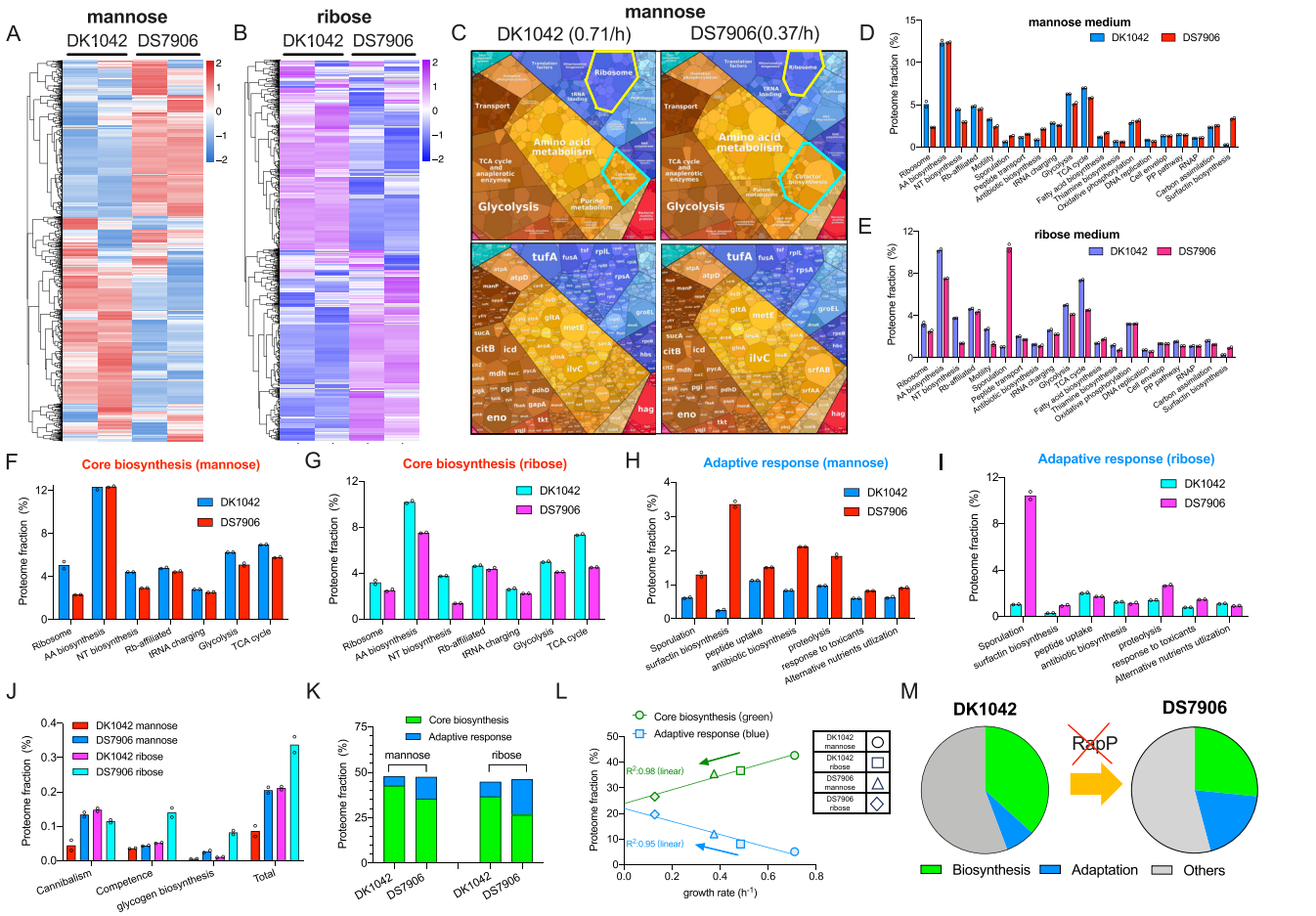

Fig. 4 | The effect of RapP on proteome allocation of *B. subtilis*. **A**, **B** Heatmaps of the proteomes of DK1042 and DS7906 strains growing in mannose and ribose media, respectively. **C** Proteome allocation of DK1042 and DS7906 strains visualized by the proteomaps website. Note that the term "mitochondrial biogenesis" inside of the large category "translation" was based on KEGG categorization consisting of both prokaryotes and eukaryotes. The readers should thus treat these proteins here as translation factors. Moreover, genes involved in biosynthesis of surfactin and some other lipopeptide antibiotics should be more properly treated as biosynthesis sector of secondary metabolites instead of cofactor biosynthesis. **D**, **E** The mass fractions of various functional proteome sectors of *B. subtilis* growing in mannose and ribose media. **F**, **G** The mass fractions of several core biosynthetic sectors of *B. subtilis* growing in mannose and ribose media. **H**, **I** The mass fractions of various adaptive response pathways of *B. subtilis* growing in mannose and ribose media. **J** The mass fractions of several low-abundant adaptive response pathways of *B. subtilis*. **K** The proteome fractions of total core biosynthetic pathways and total adaptive response pathways in mannose and ribose media. Total core biosynthetic sector refers to the sum of various sectors in (**F**) and (**G**) while total adaptive response sector refers to the sum of various sectors in (**H**–**J**). **L** The correlation of the proteome fractions of core biosynthetic category and adaptive response category with growth rates for the four conditions of *B. subtilis*. **M** Schematic illustration showing that the absence of RapP triggers the resource allocation from biosynthetic pathways to adaptive response pathways. For (**D**–**J**), individual data points correspond to two biological replicates ($n = 2$). Source data are provided as a Source Data file.

in the case of *spoOA*-null strain[27]. To see if this was the case, we conducted a two-strain fitness competitive experiment between DK1042 and DS7906 strains at two different initial mixed ratios (1:1 and 1:3) (Fig. 5A–D). In both cases, DK1042 strain gradually gained a fitness advantage over the DS7906 strain during exponential growth stages before nutrient depletion (Fig. 5B, D). Even after stationary phase when cells entered into autolysis stage[27] or during long-term starvation stage, the proportion advantage of DK1042 cells could be largely maintained in the coculture (Fig. 5B, D), suggesting that DK1042 strain did not display a fitness defect in relative to DS7906 strain during starvation stage. Therefore, we next sought to investigate the expression patterns of those adaptive response genes in DK1042 strain during different growth stages. We again measured the promoter activities of two sporulation genes, *spoIIE*, and *spoIIGA*, using LacZ reporter assay as sporulation is a key adaptive strategy of *B. subtilis* during nutrient starvation. Strikingly, the promoter activities of both genes in DK1042 strain, although being tightly repressed during growth stages (light green area in Fig. 5E, F), abruptly increased by ~200 folds after nutrient depletion (light orange area in Fig. 5E, F). In comparison, DS7906 strain exhibited a much higher leaky expressions (basal levels) of *spoIIE* and *spoIIGA* during early exponential phase (dashed line, Fig. 5G, H). Moreover, the expressions of *spoIIE* and *spoIIGA* in DS7906 strain began to increase even before nutrient depletion and finally only increased by less than 5-fold after entering into starvation stage (Fig. 5G, H). Being consistent with the gene expression patterns, DK1042 strain just exhibited a delay in entering into sporulation (red circles, Fig. 5I) compared with DS7906 strain (pink squares, Fig. 5I). Moreover, spore fractions of DK1042 strain could further increase steadily to 70% during long-term starvation stages (8 days after nutrient depletion) while the spore fractions of DS7906 strain were maintained at 70–80% (Fig. 5J). The delay of sporulation in DK1042 strain is reminiscent of the biological meaning of cannibalism of *B. subtilis*, which is beneficial for *B. subtilis* to delay or avoid the commitment to the highly energy-cost sporulation process[59,60]. Taken together, our results suggest that the presence of RapP allows the ancestral *B. subtilis* to prevent the premature expression of proteins related to adaptive response. That is, cells tightly restrict the expressions of adaptive response pathways to unleash its

https://doi.org/10.1038/s41467-024-53992-x

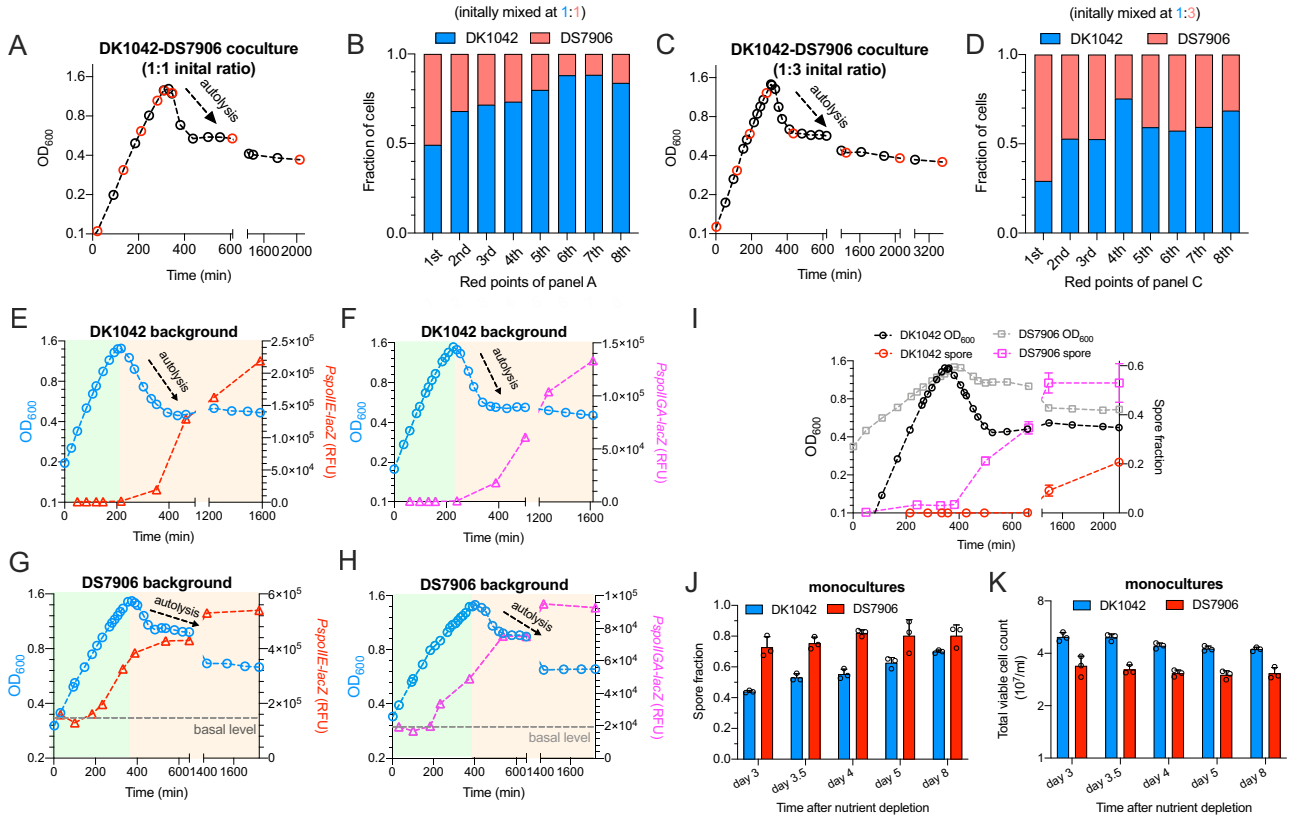

Fig. 5 | Need-based activation of sporulation pathway in the ancestral *B. subtilis*. **A** The growth curve of DK1042-DS7906 coculture in mannose minimal medium. DK1042 and DS7906 strains were initially mixed at a ratio of 1:1. **B** The relative fractions of DK1042 and DS7906 cells in the coculture of (**A**) growing in mannose minimal medium. At each red point of the growth curve in (**A**), the fractions of DK1042 and DS7906 cells in the coculture were sequentially measured by plating. The X-axis denotes the eight time points (red) throughout the growth curve of (**A**). **C**, **D** Same as (**A**, **B**) but the DK1042 and DS7906 strains were initially mixed at a ratio of 1:3. **E** The promoter activities of *spoIIE* analyzed by LacZ reporter assay at different growth stages of DK1042 strain. For (E–H), the light green area shows the growth stage before nutrient depletion. The light orange area shows the starvation stage after nutrient depletion. **F** The promoter activities of *spoIIGA* analyzed by LacZ reporter assay at different growth stages of DK1042 strain. **G** The promoter activities of *spoIIE* analyzed by LacZ reporter assay at different growth stages of DS7906 strain. **H** The promoter activities of *spoIIGA* analyzed by LacZ reporter assay at different growth stages of DS7906 strain. **I** Sporulation efficiency of DK1042 and DS7906 mono-cultures under different growth stages in mannose medium. Sporulation data are presented as the mean values ± standard deviations (SD) of three biological replicates ($n = 3$). The reference growth curves of DK1042 and DS7906 were shown, respectively. **J**, **K** The spore fractions and total viable cell counts of DK1042 and DS7906 mono-cultures during long-term starvation in mannose medium. Data points were measured on different days after nutrient depletion. The time of nutrient depletion refers to the time point when OD_{600} reaches the highest value in the growth curve. Data are presented as the mean values ± standard deviations (SD) of several biological replicates. $n = 3$ for all the data points. Source data are provided as a Source Data file.

growth potential during exponential stage while strongly activate adaptive responses after entering into starvation stage. Such an economical strategy does not compromise the long-term fitness of *B. subtilis* as we observed that DK1042 strain could maintain an even larger population size than DS7906 strain during long-term starvation after nutrient depletion (Fig. 5K).

Introduction of RapP accelerates the growth of domesticated *B. subtilis* strain

We next sought to investigate whether the introduction of RapP into domesticated *B. subtilis* strains could accelerate their growth. We constructed the RapP-complementation strains by integrating an IPTG-inducible expression cassette of *rapP* into the *amyE* locus of 168 strain and another domesticated PY79 strain (Fig. 6A). PY79 strain is a commonly used prototrophic bacterium[30,61] and exhibits similar reduced growth rates with 168 strain compared with the ancestral strain (Fig. S10). Addition of different concentrations of inducers could effectively titrate the expression of RapP in *B. subtilis* (Fig. 6A). Indeed, titrated expression of RapP strongly increased the growth rates of both 168 and PY79 strains on various carbon sources (Figs. 6B, C and S11) and enabled 168 strain to achieve comparable growth rates with DK1042 strain (Fig. 6D). We further found that RapP overexpression increased the ribosome contents (reflected by RNA/protein ratio) of 168 and PY79 strains in ribose medium (Fig. 6E). As shown in Fig. 6F, the increase of ribosome content could quantitatively explain the increase of growth rate as their relations completely overlapped with the linear relation between RNA/protein ratio and growth rate (R-line in Fig. 1D). In contrast to the trend of RNA/protein ratios, the expressions of sporulation genes (a reflection of Spo0A activity) were strongly inhibited by RapP overexpression in both 168 and PY79 strains (Fig. 6G). The growth acceleration effect of RapP disappeared in both *spo0A*-null and *spo0F*-null backgrounds (Fig. 6H, I), reinforcing the notion that RapP overexpression could accelerate cell growth via targeting the Spo0F-Spo0A signaling pathway.

We finally investigated the effect of RapP complementation on the proteome allocation of domesticated strain using mass spectrometry (Supplementary data 5–7, Figs. 7A and S12). In our condition, the RapP level in the RapP-overexpression 168 strain is almost the same as its natural level in DK1042 strain (Fig. 7B). RapP overexpression strongly re-shaped the global gene expression patterns of 168 strain (Fig. 7A) and altered the levels of various functional proteome sectors (Fig. 7C). Being consistent with the notion established in the case of ancestral strain (Fig. 4M), RapP overexpression increased the proteome investment on core biosynthetic sector

https://doi.org/10.1038/s41467-024-53992-x

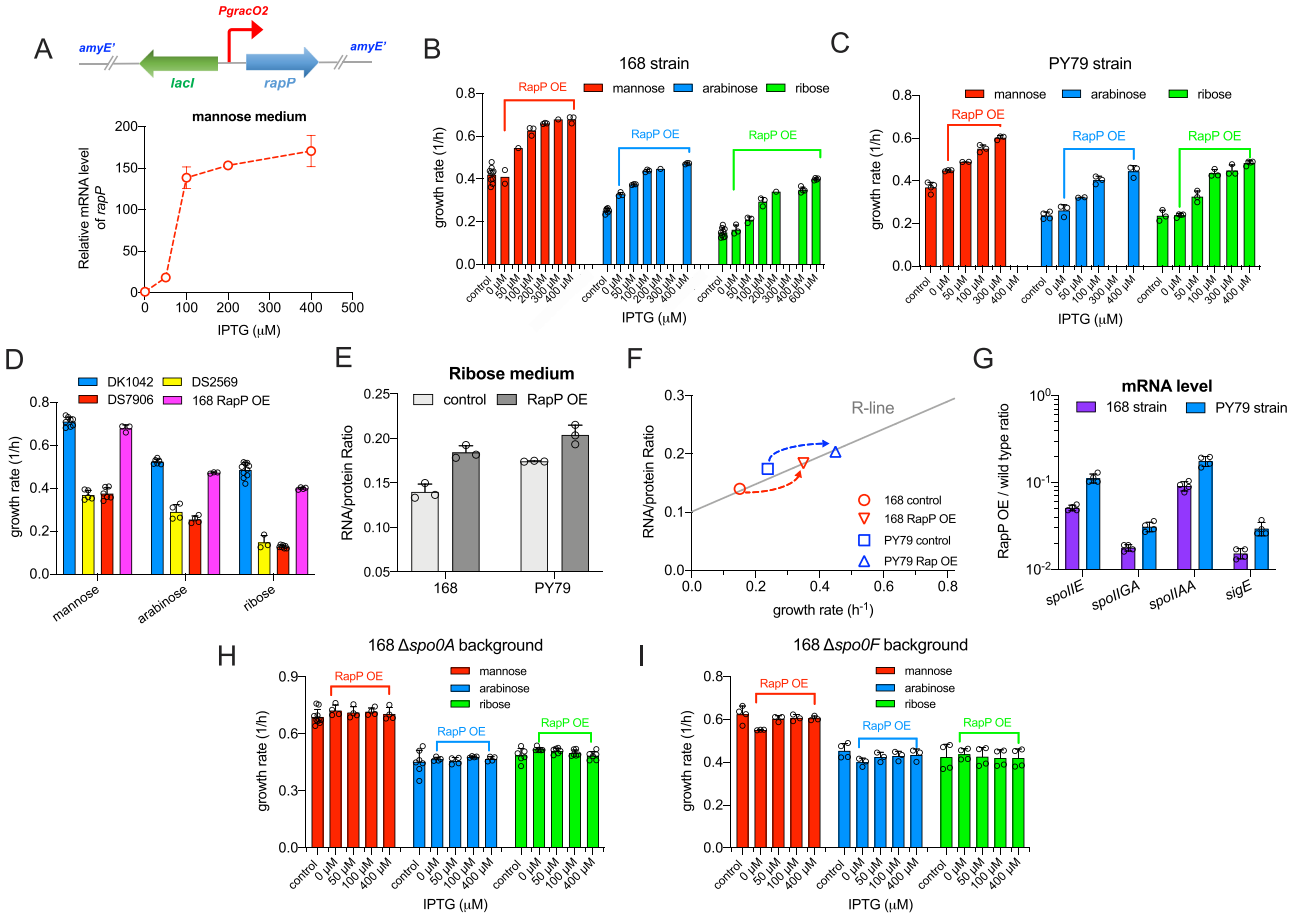

Fig. 6 | Introduction of *rapP* accelerates the growth of domesticated *B. subtilis* strains. A An IPTG-inducible *rapP* expression cassette was integrated into the *amyE* locus of the domesticated *B. subtilis* 168 and PY79 strains to obtain the *rapP*-overexpressing strains. The mRNA levels of *rapP* could be titrated by addition of different concentrations of IPTG into the medium. Data are presented as the mean values ± standard deviations (SD) of three biological replicates ($n = 3$). **B** The effect of *rapP* overexpression on the growth rates of 168 strain on different carbon sources. Control refers to wild type 168 strain. Data are presented as the mean values ± standard deviations (SD) of several biological replicates (for $n \geq 3$). For mannose medium, $n = 10, 2, 1, 3, 3, 1, 3$ for control condition, 0 μM, 50 μM, 100 μM, 200 μM, 300 μM and 400 μM IPTG, respectively; for arabinose medium, $n = 6, 3, 3, 3, 1, 3$ for control condition, 0 μM, 50 μM, 100 μM, 200 μM, 400 μM IPTG, respectively; for ribose medium, $n = 9, 3, 3, 3, 1, 4, 4$ for control condition, 0 μM, 50 μM, 100 μM, 200 μM, 400 μM and 600 μM IPTG, respectively. **C** The effect of *rapP* overexpression on the growth of PY79 strain on different carbon sources. Control refers to wild type PY79 strain. Data are presented as the mean values ± standard deviations (SD) of several biological replicates (for $n \geq 3$). For mannose medium, $n = 4, 3, 2, 3, 3$ for control condition, 0 μM, 50 μM, 100 μM and 300 μM IPTG, respectively; for arabinose medium, $n = 4, 3, 2, 3, 3$ for control condition, 0 μM, 50 μM, 100 μM, 400 μM IPTG, respectively; for ribose medium, $n = 3$ for all the conditions except for 0 μM and 400 μM IPTG conditions, in which $n = 4$. **D** The growth rates of DK1042, DS2569, DS7906, and 168 RapP-overexpressing (OE) strains on various carbon sources. The data of 168 RapP OE strain correspond to the highest values of growth rates shown in Fig. 6B. Data are presented as the mean values ± standard deviations (SD) of several biological replicates. Data of DK1042, DS2569, and DS7906 are the same as shown in Fig. 1C. For the RapP OE condition, $n = 3, 3, 4$ for mannose, arabinose, and ribose media, respectively. **E** The effect of RapP overexpression on RNA/protein ratio of 168 and PY79 strains growing in ribose medium. 400 μM and 300 μM IPTG were added to the medium of 168 and PY79 RapP-overexpressing strains, respectively. Control refers to the wild type 168 and PY79 strains. Data are presented as the mean values ± standard deviations (SD) of three biological replicates ($n = 3$). **F** The correlation of RNA/protein ratio versus growth rate for the condition of RapP overexpression. Data points correspond to the data in (**E**). The gray R-line refers to the linear fit of Fig. 1D. **G** Relative mRNA levels of four sporulation genes in wild type 168 and PY79 strains compared with their RapP OE strains in ribose medium. 400 μM IPTG was added to the medium of RapP OE strain. Data are presented as the mean values ± standard deviations (SD) of four biological replicates ($n = 4$). **H** The effect of RapP overexpression on the growth of *spo0A-null* 168 strain on different carbon sources. Control refers to *spo0A-null* 168 strain without *rapP* integration. Data are presented as the mean values ± standard deviations (SD) of several biological replicates. For the control conditions, $n = 10, 7$ in mannose and arabinose media, respectively. $n = 4$ for all the rest conditions of mannose and arabinose media. $n = 6$ for all the conditions in ribose medium. **I** The effect of *rapP* overexpression on the growth of *spo0F-null* 168 strain on different carbon sources. Control refers to *spo0F-null* 168 strain without *rapP* integration. Data are presented as the mean values ± standard deviations (SD) of several biological replicates. $n = 4$ for control conditions on all three carbon sources. For the RapP overexpression conditions, $n = 3$ for mannose and arabinose media; $n = 4$ for ribose medium. Source data are provided as a Source Data file.

(Fig. 7D) while reduced the levels of adaptive response proteins (Figs. 7E, F and S13). The increase in the level of core biosynthetic sector was quantitatively comparable with the decrease in the level of adaptive response sector (Fig. 7G). Collectively, RapP overexpression accelerates cell growth of domesticated strain by triggering a resource re-allocation from adaptive response pathway to biosynthetic pathway (illustrated in Fig. 7H).

Discussion

To thrive in nature, bacterial cells have to balance various important traits, resulting in a seemingly inevitable trade-off[19,62,63]. For example, bacteria such as *E. coli* could sense the poor nutrients as a signal of environmental deterioration based on their ecological experiences[18] so that they employ (p)ppGpp and cAMP signaling pathways to activate adaptive response at the cost of reduced biosynthetic pathways,

https://doi.org/10.1038/s41467-024-53992-x

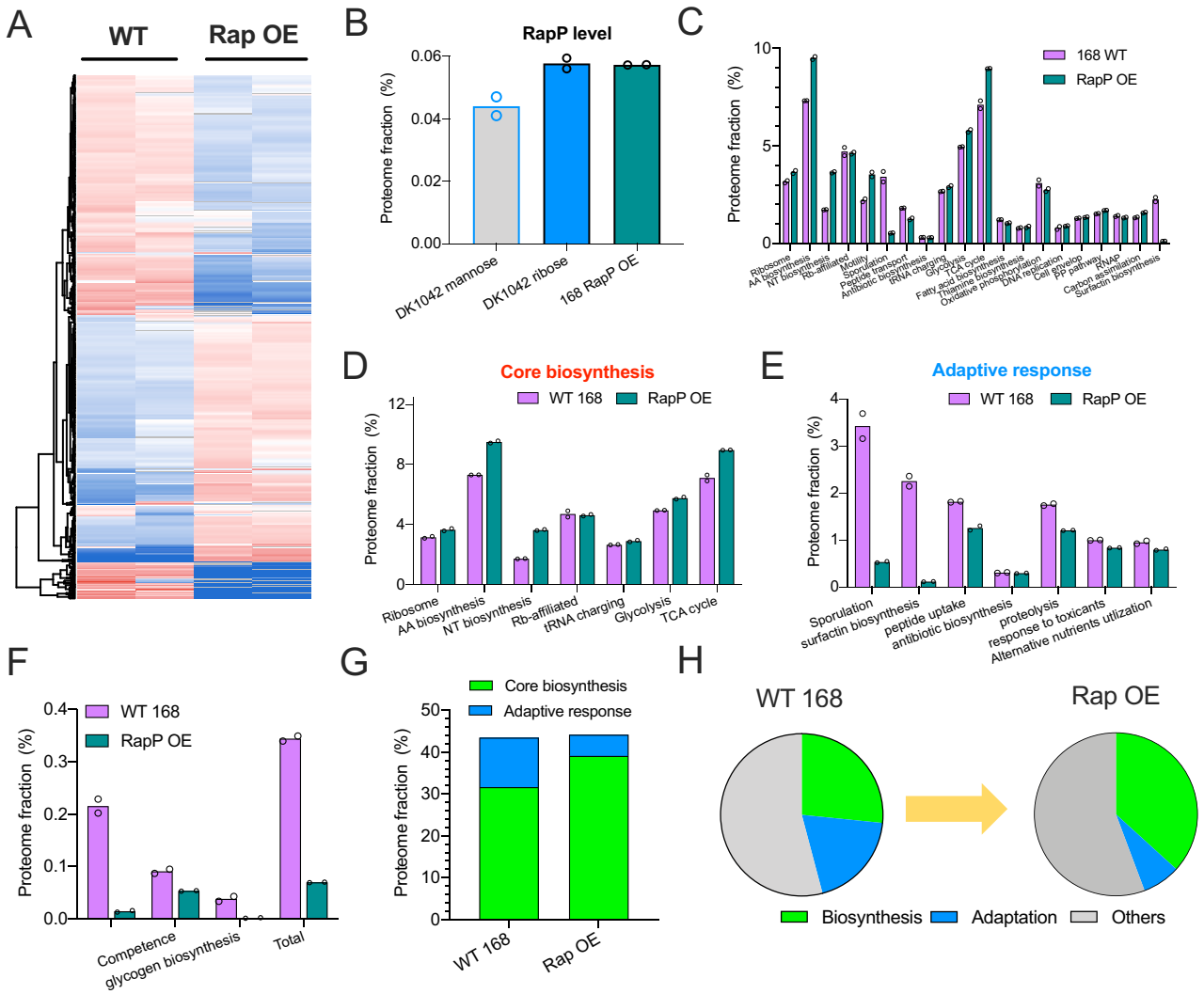

Fig. 7 | Introduction of *rapP* re-shapes the resource allocation of domesticated strain. A Heatmap of the proteomes of wild type 168 and its RapP-overexpressing (OE) strains in ribose medium. 400 μM IPTG was added to the medium of RapP-overexpressing strain. **B** The proteome fraction of RapP protein in DK1042 strain growing in mannose and ribose media and the 168 RapP OE strain growing in ribose medium. **C** The mass fractions of various functional proteome sectors. **D** The mass fractions of several core proteome sectors of biosynthesis. **E** The mass fractions of various adaptive response pathways. **F** The mass fractions of several low-abundant adaptive response pathways. **G** The proteome fractions of total core biosynthetic sector and total adaptive response sector. Total core biosynthetic sector refers to the sum of various sectors in (**D**) while total adaptive response sector refers to the sum of various sectors in (**E, F**). **H** Schematic illustration showing that RapP over-expression triggers a global resource re-allocation from adaptive response pathways to biosynthetic pathways, further accelerating the growth of domesticated strain. For (**B**–**F**), individual data points correspond to two biological replicates ($n = 2$). Source data are provided as a Source Data file.

ultimately resulting in slow growth but enhanced survivability under poor conditions[15,18,23,64]. In contrast, artificial inactivation of stress response could increase the growth rate but at the cost of reduced long-term survivability, as shown recently in the *spo0A*-null strain of *B. subtilis*[27]. Here we showed that the ancestral *B. subtilis* strain possesses an important molecular strategy of growth control, which is lost in the commonly used domesticated strains. Such strategy, mediated by a plasmid-encoded RapP protein, could effectively constrain the physiological trade-offs. RapP allows *B. subtilis* to achieve need-based regulation of resource allocation ("do the right thing at the right time") (illustrated in Fig. 8): minimizing the proteome burden of Spo0A-mediated adaptive response to unleash the growth potential during exponential stage while substantially activate them during starvation stage. Therefore, bacteria could achieve rapid growth during exponential stages without compromising the long-term fitness during late starvation stages (Fig. 5), and thus successfully addressing the growth-survival trade-off issue found in *spo0A*-null strain[27]. In contrast, *rapP*-deficient strain has an unnecessarily higher proteome burden on adaptive response even during exponential stage, which results in slower growth (Fig. 8). Therefore, although trade-off itself is fundamental, its extent could be effectively constrained by bacterial cells using sophisticated molecular strategies to reduce the direct conflicts among different objectives.

Our study has shown that RapP, by targeting the SpoOF-Spo0A signaling pathway, promotes cell growth by shifting a global resource re-allocation from adaptive pathways to biosynthetic pathways. It is known that Spo0A-P not only activates sporulation but is also required for various adaptive processes, e.g., cannibalism, biofilm formation, antibiotic biosynthesis, and competence, either via direct transcription activation[44,65] or indirect ways such as its relief of the AbrB-dependent repression[46,66]. Our data show that the presence of RapP indeed causes a global downregulation of Spo0A-mediated adaptive pathways (Figs. 4K and 7G). Nevertheless, there are still some differences among the quantitative trends of different adaptive pathways. Sporulation and several other pathways are strongly downregulated by RapP in both mannose and ribose media (Figs. 4H, I and 7E). However, there are

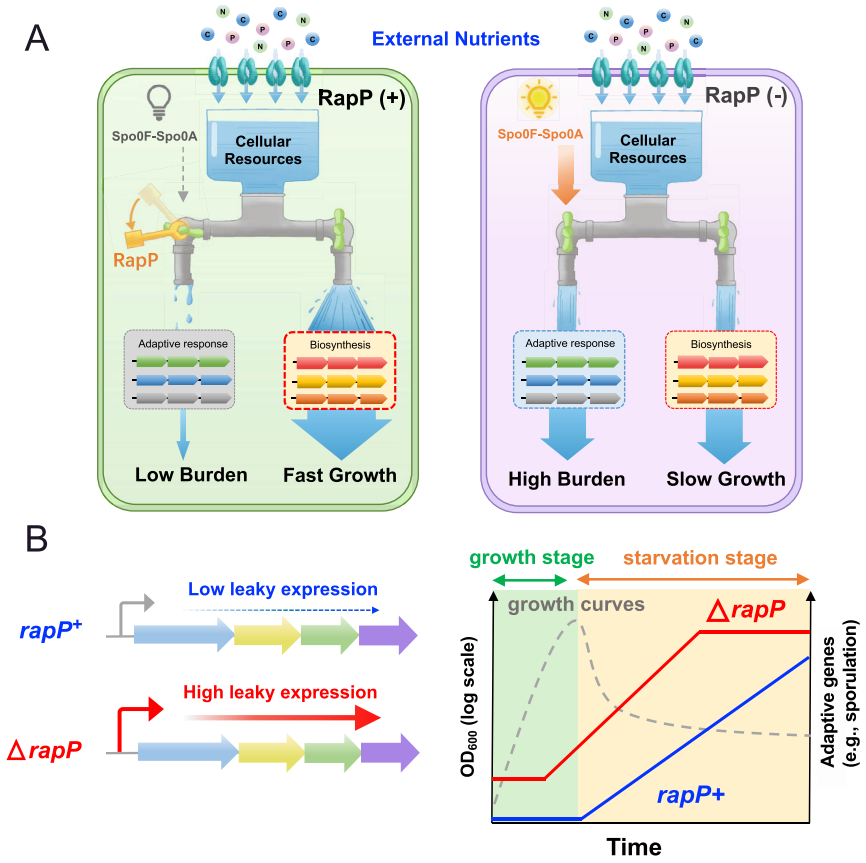

Fig. 8 | RapP protein as a global growth accelerator in *B. subtilis* and enables need-based resource allocation: a two-way faucet model. A The cellular resource is finite. RapP accelerates cell growth by minimizing the leaky expressions of Spo0A-mediated adaptive response during exponential stage and further maximizing the cellular budget of biosynthetic pathways to support rapid growth (left panel). In contrast, *rapP*-deficient strain (right panel) has an unnecessarily higher proteome burden on adaptive response even during exponential stage, which limits the cellular budget of biosynthesis and results in slower growth. **B** Schematic illustrations showing that *rapP*$^+$ ancestral strain maintains a much lower leaky expression of adaptive response pathways (e.g., sporulation) than *rapP*-null strain during exponential stage. As a result, *rapP*$^+$ ancestral strain (blue) could achieve need-based regulation of gene expression to unleash the growth potential during exponential stage while substantially activate adaptive response during starvation stage. Source data are provided as a Source Data file.

no obvious changes in the levels of biofilm-related proteins (Fig. S8). Some other adaptive pathways such as cannibalism exhibit different trends in mannose and ribose media (Fig. 4J). The underlying reason could be related to the different sensitivities of different adaptive pathways to the levels of Spo0A-P as it is known that the expressions of different adaptive pathways (e.g., sporulation, biofilm formation, competence, and cannibalism) are sensitive to different thresholds of Spo0A-P levels[44,46,65,67]. In principle, different adaptive pathways could have direct competitions for the limited numbers of cellular Spo0A-P, further affecting the relative abundances of each other, which ultimately lead to some differences in the sensitivities of various adaptive pathways to the effect of RapP. In addition, we also note that RapP could increase the levels of motility proteins (Fig. 7C), which is logical as motility genes (*fla/che* operon) are negatively regulated by Spo0A[65].

Sporulation is a highly time-consuming and energy-demanding adaptive process that is mainly triggered in *B. subtilis* when encountering long-term starvation[45,46]. Previous studies have shown that domesticated *B. subtilis* strain employs cannibalism to kill a fraction of sibling cells to obtain additional nutrient sources so that the commitment to sporulation can be avoided or delayed[46,59,60]. Our study reveals that RapP is a highly effective regulator that delays the premature entering into the energy-cost sporulation process (Fig. 5I). The *rapP*-deficient strain not only has much higher basal levels of sporulation genes but also activates the expression of sporulation genes before nutrient depletion, which is clearly not economical for *B. subtilis*. As a result, *rapP*-deficient strain enters into sporulation process much earlier than *rapP*$^+$ strain, though it contains even higher expression levels of cannibalism-related proteins in mannose medium (Fig. 4J). Therefore, RapP represents a global strategy to delay sporulation in the ancestral strain, which has been lost in the domesticated strain.

Plasmids, as major vehicles driving horizontal gene transfer (HGT), play an important role in bacterial ecology and evolution[38]. Plasmids may help bacteria to adapt to specific environments by conferring some beneficial traits, such as antimicrobial resistance, virulence, heavy metal tolerance, and utilization of alternative nutrient sources[68]. In particular, the key role of plasmids in driving the dissemination of antibiotic resistance is widely recognized[69,70]. Despite the potential benefits conferred by plasmids, plasmid carriages exert physiological burdens (metabolic and proteome costs) on hosts and are thus often associated with fitness costs, usually manifesting as reduced growth rates or weakened competitiveness[37,68]. For example, clinical pathogens expressing plasmid-encoded AmpC-type β-lactamase display reduced growth rates in drug-free conditions[69]. The fitness costs of plasmids could ultimately result in the loss of plasmids[68]. To maintain the long persistence of plasmids, bacteria could evolve compensating mutations in plasmids and chromosomes to ameliorate the plasmid cost[37,38,71]. In contrast to numerous cases of plasmid costs, here we provide a special example of plasmid carriage that could confer fitness (growth) advantage to the host cells. The positive effect of RapP in pBS32 plasmid on cell growth is substantial and broadly applicable to various carbon sources (Fig. 1), and therefore could be beneficial for the maintenance of pBS32 in *B. subtilis* in ecological niches.

A fundamental concern in the field of synthetic biology and microbial biotechnology is how to maximize the designed function, e.g., microbial bioproduction[72–74]. The trade-off between the natural functions of host cells and the synthetic circuits poses a fundamental challenge to the optimization of the designed function[72,75]. To address this issue, a promising research avenue focuses on the construction of minimal cells with streamlined genome so that unnecessary genetic elements are removed to increase the availability of cellular resources for the synthetic circuit[76,77]. For example, it has been reported that genome-reduced *B. subtilis* strain gets superior capacities in the production of foreign-secreted proteins[78]. Nevertheless, the workload of mini-genome construction is generally high and requires a systematic annotation of the essential genes[76]. Moreover, despite the tremendous efforts of constructing mini-genome strains, the success rate in improving bioproduction performance is relatively low due to unforeseeable effects on the host physiology[73,76]. Our study provides a delicate lesson of nature about how cells economize their own cellular resources for biosynthesis. The RapP allows cells to minimize the resource competition from alternative pathways so that the cellular budget for supporting biomass growth could be maximized during exponential stage. Therefore, to improve the designed functions, it is conceivable to identify and manipulate related regulators of various redundant competitive pathways so that more cellular resources are available to support the designed functions.

Methods

Strain construction

Strains used in this study included *B. subtilis* 168 strain (*trpC2*)[31], the prototrophic PY79 strain, and the ancestral NCIB 3610 strain[30]. DK1042 strain is almost genetically identical to NCIB 3610 strain except that it carries a *comI*^{Q12L} mutation in pBS32 plasmid and DS2569 strain is the NCIB 3610 strain that cured of pBS32 plasmid[36]. DS7906 strain is the *rapP*-null 3610 strain[40]. DK1042, DS2569, and DS7906 strains were kindly provided by Kearns lab. All the other strains in this study were derivatives of these parental strains.

Gene knockout of *B. subtilis* in this study was based on the double-crossover homologous recombination using the pDG1730-*Sal*I (*spc*^{R}) integration vector[27]. To construct related *spo0F*-null strain, the flanking regions of both upstream and downstream of the *spo0F* gene were PCR amplified using the genome of 168 strain as the template, being further inserted into the *Aat*II/*Bam*HI and *Eco*RV/*Sal*I sites of pDG1730-*Sal*I, respectively, generating the pDG1730-*spo0F* knockout vector. The pDG1730-*spo0F* vector was then linearized by *Xho*I digestion and transformed into related *B. subtilis* strain by natural competence for screening the spectinomycin-resistant double-crossover transformants. The *spo0A* knockout of *B. subtilis* was performed with similar procedures.

To construct the P*spoIIE-lacZ* and P*spoIIGA-lacZ* reporter strains, we used the integrated vector pAX01[79]. The *lacZ* gene of *E. coli* MG1655 was inserted into the *Bam*HI site of pAX01, generating pAX01-*lacZ* vector. The promoter regions of *spoIIE* and *spoIIGA* were PCR amplified using the genome of 168 strain as the template, being further moved into the *Xho*I/*Spe*I sites of pAX01-*lacZ* vector. The resultant *lacZ* reporter vectors were then transformed and integrated into the genome of various *B. subtilis* strains to obtain the *lacZ* reporter strains.

To construct the RapP-overexpressing domesticated strains, we first designed an artificial IPTG-inducible *PgracO2* promoter, which was derived from the *Pgrac100* promoter[80]. *PgracO2* promoter contains one more *lac* operator (lacO) to replace the original spacer region between −10 and −35 region of *Pgrac100* promoter in order to achieve much tighter regulation. The sequence of *PgracO2* is as below:

5′*agctattgtaacataatcggtacgggggtgaaaaagctaacggaaaagggagcggaaaagaatgatgtaagcgtgaaaaatttttttaaaaaatctcttgacattgtgagcggataacaatattataagaattgtggaattgtgagcggataacaattcccaattaaaggaggaa* 3′

The *PgracO2* DNA fragment (chemically synthesized by Tsingke Biotech) was inserted into the *Kpn*I/*Bam*HI sites of the pHT01 vector to replace the original *Pgrac01* promoter. The *rapP* gene was then PCR amplified using pBS32 as template. The *lacR-PgracO2* cassette in pHT01 and *rapP* gene were assembled by Gibbson assembly using Gibbson assembly kit, 2X MultiF Seamless Assembly Mix (RK21020) (ABclonal), and inserted into the *Bam*HI site of pDG1730-CmR vector, generating the pDG1730-*rapP* vector. The pDG1730-CmR was constructed by inserting the chloramphenicol resistance marker (*Cm*^{R}) cassette of pHT01 into the *Eco*RV/*Eco*RI sites to replace the original spectinomycin-resistance marker (*spc*^{R}) of pDG1730-*Sal*I (in order to facilitate the following integration to the spectinomycin-resistant *spo0A*-null and *spo0F*-null strains). The pDG1730-*rapP* was then linearized by *Xho*I and transformed into 168 or PY79 strains so that the *lacR-PgracO2-rapP* cassette was integrated into the *amyE* site of *B. subtilis*.

To facilitate the two-strain competitive experiment, the pDG1730-*Sal*I was linearized by *Xho*I and directly transformed into DK1042 strain so that the spectinomycin-resistance gene was integrated into *amyE* locus of DK1042 strain, generating the DK1042 *spc*^{R} strain.

For RapP complementation, the *PrapP-rapP* cassette (the coding region of *rapP* together with its native promoter) was PCR amplified using pBS32 plasmid as the template and further inserted into the *Nhe*I/*Bam*HI sites of pHT01 vector. The E49A mutation was introduced directly by PCR-mediated mutagenesis approach combined with *Dpn*I digestion[81].

Growth medium

B. subtilis was cultured in either LB broth or modified C-minimal medium[82]. The basic recipe of C-minimal medium is as below: 16 g/L K_2HPO_4, 4 g/L KH_2PO_4, 2.32 mg/L $MnSO_4{\cdot}4H_2O$, 0.123 g/L $MgSO_4{\cdot}7H_2O$, 12.5 μM $ZnCl_2$, 50 mg/L tryptophan, and 22 mg/L ferric ammonium citrate. 20 mM NH_4Cl was used as the nitrogen source. Carbon sources used were one of the following: 0.4% glucose, 0.4% mannose, 0.4% arabinose, or 0.4% ribose. The glucose plus casamino acids (cAA) medium contained 0.4% casamino acid and 0.4% glucose.

Cell growth procedures

Batch culture growth of *B. subtilis* was performed either in an air bath shaker or a water bath shaker (200 rpm, 37 °C). A standard cell culturing procedure contained three steps: seed culture, pre-culture, and final experimental culture. For seed culture, cells from a fresh colony were inoculated first into LB broth (Coolaber, Beijing) and grew several hours to $OD_{600} > 1$. For pre-culture, the seed culture was washed and transferred into the C-minimal medium for growing overnight. On the next day, the overnight pre-culture was inoculated into the same C-minimal medium at an initial OD_{600} of ~0.02 as the final experimental culture (if the overnight pre-culture was still within exponential growth stage at OD_{600} from 0.2 to 0.6; then the final culture could be initiated at a high initial OD. The growth curve was manually measured using a Genesys 50 spectrophotometer (Thermo Fisher Scientific). 5–8 OD_{600} data points (usually within the range of 0.05–0.5) were measured to obtain the exponential growth curve for calculating growth rate. Growth curves were alternatively measured using an Agilent Biotek Synergy H1 microplate reader.

β-galactosidase (LacZ) reporter assay

Due to low activities of *PspoIIE-lacZ* and *PspoIIG-lacZ* reporter, we used a sensitive fluorescence substrate 4-methylumbelliferyl-D-galactopyranoside (MUG, purchased from GLPBIO)[43] in order to detect the low activity of β-galactosidase. In brief, 50–200 μl cell sample was supplemented with Z-buffer (with 200 μg/mL chloramphenicol) to a final volume of 400 μl. 50 μl of 3 mg/mL MUG was then added to initiate the reaction process. 180 μl reaction mixtures were then immediately transferred to a costar black 96-well plate and

subject to kinetic measurement for 2–4 h using an Agilent Biotek Synergy H1 microplate reader (Ex/Em: 360 nm/460 nm). The slope of the linear fit of the time-course fluorescence intensity (normalized by the volume of cell sample) was used as an indicator of the LacZ activity.

Measurement of RNA/protein ratio

To obtain the RNA/protein ratio of *B. subtilis*, we measured both the total RNA content and total protein content of exponentially growing *B. subtilis* cultures. The determination of total RNA was based on the perchloric acid ($HClO_4$) and potassium hydroxide (KOH) treatment method while determination of total protein were based on the Bicinchoninic acid assay (BCA), which was performed as described in You et al.[83].

Two-strain competitive experiment

The overnight mono-cultures of DK1042 (spc^R) strain (with *spcR* integrated at the *amyE* locus of DK1042 strain) and DS7906 strain in mannose medium were grown to exponential stages ($OD_{600}\approx0.5$), being then mixed at a ratio of 1:1 or 1:3 and further inoculated into the same minimal medium at an initial $OD_{600}\approx 0.1$. Throughout the process of competitive experiment, the growth of the coculture was monitored using a Genesys 50 spectrophotometer (Thermo Sci). At different growth stages, 0.3 mL cell sample was taken and subject to serial dilution. The properly diluted sample was pipetted into two types of LB agar: one supplied with 100 μg/mL spectinomycin for determining the cell count of DK1042 strain in the coculture; another drug-free agar for determining the total cell count of the coculture.

Sporulation efficiency

The sporulation efficiency of *B. subtilis* was assayed by the heat shock method[84]. At each time point, two 0.3 mL cell samples from the same *B. subtilis* cultures were taken: one sample was directly subject to serial dilutions for measuring the total cell count, N_{total}. Meanwhile, the other sample was subject to heat treatment under 80 °C for 20 min to kill the vegetative cells but retain the spores. The heat-treated sample was then also serially diluted to get the count of spores, N_{spore}. The sporulation efficiency equals to N_{spore}/N_{total}.

mRNA level determination by qRT-PCR

Determination of mRNA levels such as *spoIIE, spoIIGA, spoIIAA, sigE*, and *rapP* was based on qRT-PCR method as similarly described in Zhu et al.[85]. 0.8 mL exponentially growing culture of *B. subtilis* ($OD_{600}\approx0.4$) was added to 1 mL cold stop solution (60% ethanol, 2% phenol, 10 mM EDTA, and 10 μg/mL actinomycin D) in a 2 mL centrifuge tube. The fixed cells were then pelleted for RNA extraction using a bacterial RNA extraction kit (TianGen Biotech, Beijing). cDNA synthesis was then performed with first-strand cDNA synthesis reverse transcriptase kit (TianGen). The qRT-PCR reaction was performed in an ABI QuantStudio 3 real-time Thermocycler using the Hieff® qPCR SYBR Green Master Mix (Yeasen Biotech) according to the manual. The PCR reaction procedure was as follows: 95 °C for 5 min, followed by 40 cycles of 95 °C for 10 s, 60 °C for 20 s and 72 °C for 30 s.

Proteomics

The proteomics method was based on 4D label-free mass spectrometry as described in Zhu et al.[27] and provided again as below: 40 mL exponentially growing culture of *B. subtilis* ($OD600\approx0.4$) was transferred into a pre-cooled 50 mL centrifuge tube, and collected by centrifugation (4 °C, 8000 × *g* for 5 min). The cell pellets were washed twice by PBS, dried by a speed vacuum concentrator (CV600, Beijing JM Technology Co., Ltd.), and stored at −80 °C freezer prior to proteomic analysis. The 4D label-free proteomic experiment[51] was performed by Jingjie PTM Biolabs (Hang Zhou). For details: the cell pellets were first subject to ultra-sonication in lysis buffer (8 M Urea 8 M urea, 1% Triton X-100, 10 mM DTT, 1% protease inhibitor cocktail, and 2 mM EDTA). The cell debris was then removed by centrifugation (4 °C, 12,000 × *g* for 10 min) and the supernatant was transferred into a new centrifuge tube for measuring protein concentrations using BCA kit. Protein samples were next pelleted by 20% TCA at 4 °C for 2 h and then collected by centrifugation (4500 g/min) for 5 min. The precipitates were washed twice by pre-cooled acetone and further supplemented with 200 mM TEAB. Trypsin was then added at 1:50 trypsin-to-protein mass ratio for digestion overnight. The solution was further reduced with 5 mM DTT for 30 min at 56 °C and alkylated with 11 mM iodoacetamide for 15 min at room temperature in darkness. Finally, the peptides were desalted by C18 SPE column. Solvent A (0.1% formic acid, 2% acetonitrile) and Solvent B (0.1% formic acid, 100% acetonitrile) were then used for the following peptides separation and UPLC procedures. The peptides were dissolved in solvent A and separated by the NanoElute UPLC system. The flow setting of UPLC was as follows: 0–43 min, 6% ~ 22%B; 43–55 min, 22% ~ 30%B; 55–58 min, 30% ~ 80%B; 58–61 min, 80%B; flow rate: 450 nl/min. After UPLC separation, the peptide was set into Capillary ionization source for ionization and further analyzed by timsTOF Pro mass spectrometry system. The electrospray voltage applied was set at 1.6–1.8 kV. Both the original peptide ion and its secondary fragments were detected and analyzed by high-resolution TOF. The m/z scan range was 100–1700 for full scan. Precursors with charge states 0–5 were selected for fragmentation, and 10 PASEF-MS/MS scans were acquired per cycle. The dynamic exclusion was set to 30 s. The mass spectra data were searched against the SwissProt *Bacillus subtilis* 168 databases (plus the annotation information of pBS32 plasmid) and analyzed by Maxquant v1.6.15.0 software[86], which gave the information of both LFQ intensity and iBAQ intensity. The relative abundance of each protein across conditions was indicated by LFQ intensity. The mass proteome fraction (absolute abundance) of individual proteins was obtained using the iBAQ intensity of each protein to multiply the molecular weight (MW) (referred to as "iBAQ mass" in supplementary data) and further normalized by the sum of the whole proteome (as iBAQ is a proxy of the copy number)[87]. The iBAQ mass of individual proteins was submitted to proteomaps website (https://proteomaps.net) to obtain the KEGG resource allocation map of *B. subtilis* cells[52].

Reporting summary

Further information on research design is available in the Nature Portfolio Reporting Summary linked to this article.

Data availability

The mass spectrometry proteomics data have been deposited to the ProteomeXchange Consortium via the PRIDE partner repository with the dataset identifier PXD053191 for XA1826LQ project and PXD053195 for XA1827LQ project. The core data of proteomics related to Fig. 4, Fig. 7, and related supplementary figures are provided also in Supplementary Data 1–7. Source Data are provided with this paper.

References

1. Scott, M. & Hwa, T. Shaping bacterial gene expression by physiological and proteome allocation constraints. *Nat. Rev. Microbiol.* **21**, 327–342 (2022).
2. Scott, M., Gunderson, C. W., Mateescu, E. M., Zhang, Z. & Hwa, T. Interdependence of cell growth and gene expression: origins and consequences. *Science* **330**, 1099–1102 (2010).
3. Reyes-Lamothe, R. & Sherratt, D. J. The bacterial cell cycle, chromosome inheritance and cell growth. *Nat. Rev. Microbiol.* **17**, 467–478 (2019).
4. Belliveau, N. M. et al. Fundamental limits on the rate of bacterial growth and their influence on proteomic composition. *Cell Syst.* **12**, 924–944.e922 (2021).

5. Kostinski, S. & Reuveni, S. Ribosome composition maximizes cellular growth rates in *E. coli*. *Phys. Rev. Lett.* **125**, 028103 (2020).
6. Jorgensen, B. B. & Boetius, A. Feast and famine—microbial life in the deep-sea bed. *Nat. Rev. Microbiol.* **5**, 770–781 (2007).
7. Holscher, H. D. The gut microbiome in feast and famine. *Nat. Rev. Gastroenterol. Hepatol.* **18**, 749–750 (2021).
8. Wu, C. et al. Enzyme expression kinetics by Escherichia coli during transition from rich to minimal media depends on proteome reserves. *Nat. Microbiol.* **8**, 347–359 (2023).
9. Zhu, M. & Dai, X. Stringent response ensures the timely adaptation of bacterial growth to nutrient downshift. *Nat. Commun.* **14**, 467 (2023).
10. Basan, M. et al. A universal trade-off between growth and lag in fluctuating environments. *Nature* **584**, 470–474 (2020).
11. Hengge, R. Stationary-phase gene regulation in Escherichia coli. *EcoSal Plus* **4**, https://doi.org/10.1128/ecosalplus.5.6.3 (2011).
12. Irving, S. E., Choudhury, N. R. & Corrigan, R. M. The stringent response and physiological roles of (pp)pGpp in bacteria. *Nat. Rev. Microbiol.* **19**, 256–271 (2021).
13. Roop, J. I., Chang, K. C. & Brem, R. B. Polygenic evolution of a sugar specialization trade-off in yeast. *Nature* **530**, 336–339 (2016).
14. Levin-Reisman, I. et al. Antibiotic tolerance facilitates the evolution of resistance. *Science* **355**, 826–830 (2017).
15. Biselli, E., Schink, S. J. & Gerland, U. Slower growth of Escherichia coli leads to longer survival in carbon starvation due to a decrease in the maintenance rate. *Mol. Syst. Biol.* **16**, e9478 (2020).
16. Balakrishnan, R., de Silva, R. T., Hwa, T. & Cremer, J. Suboptimal resource allocation in changing environments constrains response and growth in bacteria. *Mol. Syst. Biol.* **17**, e10597 (2021).
17. Şimşek, E. & Kim, M. The emergence of metabolic heterogeneity and diverse growth responses in isogenic bacterial cells. *ISME J.* **12**, 1199–1209 (2018).
18. Mukherjee, A. et al. Plasticity of growth laws tunes resource allocation strategies in bacteria. *PLoS Comput. Biol.* **20**, e1011735 (2024).
19. Zhu, M. & Dai, X. Shaping of microbial phenotypes by trade-offs. *Nat. Commun.* **15**, 4238 (2024).
20. Battesti, A., Majdalani, N. & Gottesman, S. The RpoS-mediated general stress response in *Escherichia coli*. *Annu. Rev. Microbiol.* **65**, 189–213 (2011).
21. Maharjan, R. et al. The form of a trade-off determines the response to competition. *Ecol. Lett.* **16**, 1267–1276 (2013).
22. Abram, F., Arcari, T., Guerreiro, D. & O'Byrne, C. P. Evolutionary trade-offs between growth and survival: the delicate balance between reproductive success and longevity in bacteria. *Adv. Microb. Physiol.* **79**, 133–162 (2021).
23. Zhu, M., Mu, H. & Dai, X. Integrated control of bacterial growth and stress response by (p)ppGpp in Escherichia coli: a seesaw fashion. *iScience* **27**, 108818 (2024).
24. Balakrishnan, R. & Cremer, J. Conditionally unutilized proteins and their profound effects on growth and adaptation across microbial species. *Curr. Opin. Microbiol.* **75**, 102366 (2023).
25. Gude, S. et al. Bacterial coexistence driven by motility and spatial competition. *Nature* **578**, 588–592 (2020).
26. Sun, Y., Hürlimann, S. & Garner, E. Growth rate is modulated by monitoring cell wall precursors in Bacillus subtilis. *Nat. Microbiol.* **8**, 469–480 (2023).
27. Zhu, M. et al. A fitness trade-off between growth and survival governed by Spo0A-mediated proteome allocation constraints in Bacillus subtilis. *Sci. Adv.* **9**, eadg9733 (2023).
28. La Rosa, R., Rossi, E., Feist, A. M., Johansen, H. K. & Molin, S. Compensatory evolution of Pseudomonas aeruginosa's slow growth phenotype suggests mechanisms of adaptation in cystic fibrosis. *Nat. Commun.* **12**, 3186 (2021).
29. Baek, S. H., Li, A. H. & Sassetti, C. M. Metabolic regulation of mycobacterial growth and antibiotic sensitivity. *PLoS Biol.* **9**, e1001065 (2011).
30. Zeigler, D. R. et al. The origins of 168, W23, and other *Bacillus subtilis* legacy strains. *J. Bacteriol.* **190**, 6983–6995 (2008).
31. Kunst, F. et al. The complete genome sequence of the gram-positive bacterium Bacillus subtilis. *Nature* **390**, 249–256 (1997).
32. Pedreira, T., Elfmann, C. & Stülke, J. The current state of SubtiWiki, the database for the model organism Bacillus subtilis. *Nucleic Acids Res.* **50**, D875–d882 (2022).
33. Bremer, E. et al. A model industrial workhorse: Bacillus subtilis strain 168 and its genome after a quarter of a century. *Micro. Biotechnol.* **16**, 1203–1231 (2023).
34. McLoon, A. L., Guttenplan, S. B., Kearns, D. B., Kolter, R. & Losick, R. Tracing the domestication of a biofilm-forming bacterium. *J. Bacteriol.* **193**, 2027–2034 (2011).
35. Burton, A. T. & Kearns, D. B. The large pBS32/pLS32 plasmid of ancestral Bacillus subtilis. *J. Bacteriol.* **202**, https://doi.org/10.1128/jb.00290-20 (2020).
36. Konkol, M. A., Blair, K. M. & Kearns, D. B. Plasmid-encoded ComI inhibits competence in the ancestral 3610 strain of *Bacillus subtilis*. *J. Bacteriol.* **195**, 4085–4093 (2013).
37. San Millan, A. & MacLean, R. C. Fitness costs of plasmids: a limit to plasmid transmission. *Microbiol. Spectr.* **5**, https://doi.org/10.1128/microbiolspec.MTBP-0016-2017 (2017).
38. Rodríguez-Beltrán, J., DelaFuente, J., León-Sampedro, R., MacLean, R. C. & San Millán, Á. Beyond horizontal gene transfer: the role of plasmids in bacterial evolution. *Nat. Rev. Microbiol.* **19**, 347–359 (2021).
39. Nordgaard, M., Mortensen, R. M. R., Kirk, N. K., Gallegos-Monterrosa, R. & Kovács, Á.T. Deletion of Rap-Phr systems in Bacillus subtilis influences in vitro biofilm formation and plant root colonization. *MicrobiologyOpen* **10**, e1212 (2021).
40. Parashar, V., Konkol, M. A., Kearns, D. B. & Neiditch, M. B. A plasmid-encoded phosphatase regulates Bacillus subtilis biofilm architecture, sporulation, and genetic competence. *J. Bacteriol.* **195**, 2437–2448 (2013).
41. Dai, X. & Zhu, M. Coupling of ribosome synthesis and translational capacity with cell growth. *Trends Biochem. Sci.* **45**, 681–692 (2020).
42. Li, G. W., Burkhardt, D., Gross, C. & Weissman, J. S. Quantifying absolute protein synthesis rates reveals principles underlying allocation of cellular resources. *Cell* **157**, 624–635 (2014).
43. Dai, X. et al. Reduction of translating ribosomes enables *Escherichia coli* to maintain elongation rates during slow growth. *Nat. Microbiol.* **2**, 16231 (2016).
44. Piggot, P. J. & Hilbert, D. W. Sporulation of Bacillus subtilis. *Curr. Opin. Microbiol.* **7**, 579–586 (2004).
45. Higgins, D. & Dworkin, J. Recent progress in *Bacillus subtilis* sporulation. *FEMS Microbiol. Rev.* **36**, 131–148 (2012).
46. González-Pastor, J. E. Cannibalism: a social behavior in sporulating *Bacillus subtilis*. *FEMS Microbiol. Rev.* **35**, 415–424 (2011).
47. Cairns, L. S., Hobley, L. & Stanley-Wall, N. R. Biofilm formation by Bacillus subtilis: new insights into regulatory strategies and assembly mechanisms. *Mol. Microbiol.* **93**, 587–598 (2014).
48. Omer Bendori, S., Pollak, S., Hizi, D. & Eldar, A. The RapP-PhrP quorum-sensing system of Bacillus subtilis strain NCIB3610 affects biofilm formation through multiple targets, due to an atypical signal-insensitive allele of RapP. *J. Bacteriol.* **197**, 592–602 (2015).
49. Pollak, S., Omer Bendori, S. & Eldar, A. A complex path for domestication of B. subtilis sociality. *Curr. Genet.* **61**, 493–496 (2015).
50. Mirouze, N., Prepiak, P. & Dubnau, D. Fluctuations in spo0A transcription control rare developmental transitions in Bacillus subtilis. *PLoS Genet.* **7**, e1002048 (2011).

51. Meier, F. et al. Online parallel accumulation–serial fragmentation (PASEF) with a novel trapped ion mobility mass spectrometer. *Mol. Cell. Proteom.* **17**, 2534–2545 (2018).
52. Liebermeister, W. et al. Visual account of protein investment in cellular functions. *Proc. Natl. Acad. Sci. USA* **111**, 8488–8493 (2014).
53. Kalamara, M., Spacapan, M., Mandic-Mulec, I. & Stanley-Wall, N. R. Social behaviours by *Bacillus subtilis*: quorum sensing, kin discrimination and beyond. *Mol. Microbiol.* **110**, 863–878 (2018).
54. Harwood, C. R., Mouillon, J. M., Pohl, S. & Arnau, J. Secondary metabolite production and the safety of industrially important members of the *Bacillus subtilis* group. *FEMS Microbiol. Rev.* **42**, 721–738 (2018).
55. Basan, M. et al. Overflow metabolism in *Escherichia coli* results from efficient proteome allocation. *Nature* **528**, 99–104 (2015).
56. Klumpp, S., Scott, M., Pedersen, S. & Hwa, T. Molecular crowding limits translation and cell growth. *Proc. Natl. Acad. Sci. USA* **110**, 16754–16759 (2013).
57. Hamoen, L. W., Venema, G. & Kuipers, O. P. Controlling competence in Bacillus subtilis: shared use of regulators. *Microbiology* **149**, 9–17 (2003).
58. Preiss, J. Glycogen: biosynthesis and regulation. *EcoSal Plus* **6**, https://doi.org/10.1128/ecosalplus.ESP-0015-2014 (2014).
59. González-Pastor, J. E., Hobbs, E. C. & Losick, R. Cannibalism by sporulating bacteria. *Science* **301**, 510–513 (2003).
60. Ellermeier, C. D., Hobbs, E. C., Gonzalez-Pastor, J. E. & Losick, R. A three-protein signaling pathway governing immunity to a bacterial cannibalism toxin. *Cell* **124**, 549–559 (2006).
61. Schroeder, J. W. & Simmons, L. A. Complete genome sequence of Bacillus subtilis strain PY79. *Genome Announc.* **1**, https://doi.org/10.1128/genomeA.01085-13 (2013).
62. Weiße, A. Y., Oyarzún, D. A., Danos, V. & Swain, P. S. Mechanistic links between cellular trade-offs, gene expression, and growth. *Proc. Natl. Acad. Sci. USA* **112**, E1038–E1047 (2015).
63. Huang, Y., Mukherjee, A., Schink, S., Benites, N. C. & Basan, M. Evolution and stability of complex microbial communities driven by trade-offs. *Mol. Syst. Biol.* https://doi.org/10.1038/s44320-024-00051-8 (2024).
64. Phaiboun, A., Zhang, Y., Park, B. & Kim, M. Survival kinetics of starving bacteria is biphasic and density-dependent. *PLoS Comput. Biol.* **11**, e1004198 (2015).
65. Fujita, M., González-Pastor, J. E. & Losick, R. High- and low-threshold genes in the Spo0A regulon of Bacillus subtilis. *J. Bacteriol.* **187**, 1357–1368 (2005).
66. Phillips, Z. E. & Strauch, M. A. Bacillus subtilis sporulation and stationary phase gene expression. *Cell Mol. Life Sci.* **59**, 392–402 (2002).
67. Mirouze, N., Desai, Y., Raj, A. & Dubnau, D. Spo0A~P imposes a temporal gate for the bimodal expression of competence in Bacillus subtilis. *PLoS Genet.* **8**, e1002586 (2012).
68. Carroll, A. C. & Wong, A. Plasmid persistence: costs, benefits, and the plasmid paradox. *Can. J. Microbiol.* **64**, 293–304 (2018).
69. Andersson, D. I. & Hughes, D. Antibiotic resistance and its cost: is it possible to reverse resistance? *Nat. Rev. Microbiol.* **8**, 260–271 (2010).
70. Castañeda-Barba, S., Top, E. M. & Stalder, T. Plasmids, a molecular cornerstone of antimicrobial resistance in the One Health era. *Nat. Rev. Microbiol.* **22**, 18–32 (2024).
71. Brockhurst, M. A. & Harrison, E. Ecological and evolutionary solutions to the plasmid paradox. *Trends Microbiol.* **30**, 534–543 (2022).
72. Hidalgo, D. & Utrilla, J. in *Minimal Cells: Design, Construction, Biotechnological Applications* (eds Lara, A. R. & Gosset, G.) 211–230 (Springer International Publishing, 2020).
73. Noack, S. & Baumgart, M. Communities of niche-optimized strains: small-genome organism consortia in bioproduction. *Trends Biotechnol.* **37**, 126–139 (2019).
74. Stone, A., Youssef, A., Rijal, S., Zhang, R. & Tian, X. J. Context-dependent redesign of robust synthetic gene circuits. *Trends Biotechnol.* https://doi.org/10.1016/j.tibtech.2024.01.003 (2024).
75. Liao, C., Blanchard, A. E. & Lu, T. An integrative circuit-host modelling framework for predicting synthetic gene network behaviours. *Nat. Microbiol.* **2**, 1658–1666 (2017).
76. Xu, X. et al. Trimming the genomic fat: minimising and re-functionalising genomes using synthetic biology. *Nat. Commun.* **14**, 1984 (2023).
77. Kim, K., Choe, D., Cho, S., Palsson, B. & Cho, B. K. Reduction-to-synthesis: the dominant approach to genome-scale synthetic biology. *Trends Biotechnol.* https://doi.org/10.1016/j.tibtech.2024.02.008 (2024).
78. Aguilar Suárez, R., Stülke, J. & van Dijl, J. M. Less is more: toward a genome-reduced bacillus cell factory for "difficult proteins". *ACS Synth. Biol.* **8**, 99–108 (2019).
79. Härtl, B., Wehrl, W., Wiegert, T., Homuth, G. & Schumann, W. Development of a new integration site within the *Bacillus subtilis* chromosome and construction of compatible expression cassettes. *J. Bacteriol.* **183**, 2696 (2001).
80. Phan, T. T., Tran, L. T., Schumann, W. & Nguyen, H. D. Development of Pgrac100-based expression vectors allowing high protein production levels in Bacillus subtilis and relatively low basal expression in Escherichia coli. *Microb. Cell Fact.* **14**, 72 (2015).
81. Zheng, L., Baumann, U. & Reymond, J. L. An efficient one-step site-directed and site-saturation mutagenesis protocol. *Nucleic Acids Res.* **32**, e115 (2004).
82. Commichau, F. M., Gunka, K., Landmann, J. J. & Stulke, J. Glutamate metabolism in Bacillus subtilis: gene expression and enzyme activities evolved to avoid futile cycles and to allow rapid responses to perturbations of the system. *J. Bacteriol.* **190**, 3557–3564 (2008).
83. You, C. et al. Coordination of bacterial proteome with metabolism by cyclic AMP signalling. *Nature* **500**, 301–306 (2013).
84. Chen, Z. et al. *Bacillus subtilis* histidine kinase KinC activates biofilm formation by controlling heterogeneity of single-cell responses. *mBio* **13**, e0169421 (2022).
85. Zhu, M., Mu, H., Han, F., Wang, Q. & Dai, X. Quantitative analysis of asynchronous transcription-translation and transcription processivity in *Bacillus subtilis* under various growth conditions. *iScience* **24**, 103333 (2021).
86. Tyanova, S., Temu, T. & Cox, J. The MaxQuant computational platform for mass spectrometry-based shotgun proteomics. *Nat. Protoc.* **11**, 2301–2319 (2016).
87. Tomáš et al. Quantitative insights into the cyanobacterial cell economy. *eLife* **8**, e42508 (2019).

Acknowledgements

This work was supported by the National Natural Science Foundation of China 32270034 (Z.M.), 32370044 (D.X.), 32470038 (Z.M.), the National Key Research and Development Program of China 2022YFF1000400 (D.X.), Changjiang Young Scholar Program of Chinese Ministry of Education (D.X.), Natural Science Funds for Distinguished Young Scholar of Hubei Province 2022CFA044 (Z.M.), Wuhan Science and Technology Major Project 2023020302020708 (D.X.) and the Fundamental Research Funds for the Central Universities (D.X. and Z.M.).

Author contributions

D.X. conceptualized this study. D.X. and Z.M. designed the experimental flow of the whole study. Z.M., D.X., W.Y., M.H., H.F., W.Q., P.Y., W.X. performed experiments. D.X. and Z.M. analyzed data, wrote, and revised the manuscript.

Competing interests

The authors declare no competing interests.

Additional information

Supplementary information The online version contains supplementary material available at https://doi.org/10.1038/s41467-024-53992-x.

Correspondence and requests for materials should be addressed to Xiongfeng Dai.

Peer review information *Nature Communications* thanks Jörg Stülke and the other, anonymous, reviewers for their contribution to the peer review of this work. A peer review file is available.